

Structure and material study of dielectric laser accelerators based on the inverse Cherenkov effect

Bin Sun(孙斌), Yang-Fan He(何阳帆), Ruo-Yun Luo(罗若云), Tai-Yang Zhang(章太阳), Qiang Zhou(周强), Shao-Yi Wang(王少义), Du Wang(王度), and Zong-Qing Zhao(赵宗清)

Citation: Chin. Phys. B, 2023, 32 (**9**): 094101. DOI: 10.1088/1674-1056/acdc0a
Journal homepage: http://cpb.iphy.ac.cn; http://iopscience.iop.org/cpb

What follows is a list of articles you may be interested in

Particle-in-cell simulations of low-β magnetic reconnection driven by laser interaction with a capacitor-coil target

Xiaoxia Yuan(原晓霞), Cangtao Zhou(周沧涛), Hua Zhang(张华), Ran Li(李然), Yongli Ping(平永利), and Jiayong Zhong(仲佳勇)

Chin. Phys. B, 2023, 32 (**5**): 054101. DOI: 10.1088/1674-1056/acb911

Plasma density transition-based electron injection in laser wake field acceleration driven by a flying focus laser

Pan-Fei Geng(耿盼飞), Min Chen(陈民), Xiang-Yan An(安相炎), Wei-Yuan Liu(刘维媛), Xin-Zhe Zhu(祝昕哲), Jian-Long Li(李建龙), Bo-Yuan Li(李博原), and Zheng-Ming Sheng(盛政明)

Chin. Phys. B, 2023, 32 (**4**): 044101. DOI: 10.1088/1674-1056/acae79

Generation of laser-driven flyer dominated by shock-induced shear bands: A molecular dynamics simulation study

Deshen Geng(耿德珅), Danyang Liu(刘丹阳), Jianying Lu(鲁建英), Chao Chen(陈超), Junying Wu(伍俊英), Shuzhou Li(李述周), and Lang Chen(陈朗)

Chin. Phys. B, 2022, 31 (**2**): 024101. DOI: 10.1088/1674-1056/ac2f2d

Terahertz radiation generation by beating of two chirped laser pulses in a warm collisional magnetized plasma

Motahareh Arefnia, Mehdi Sharifian, and Mohammad Ghorbanalilu

Chin. Phys. B, 2021, 30 (**9**): 094101. DOI: 10.1088/1674-1056/abfb5d

Direct electron acceleration by chirped laser pulse in a cylindrical plasma channel

Yong-Nan Hu(胡永南), Li-Hong Cheng(成丽红), Zheng-Wei Yao(姚征伟), Xiao-Bo Zhang(张小波), Ai-Xia Zhang(张爱霞), Ju-Kui Xue(薛具奎)

Chin. Phys. B, 2020, 29 (**8**): 084103. DOI: 10.1088/1674-1056/ab943d

---

Structure and material study of dielectric laser accelerators based on the inverse Cherenkov effect

Bin Sun(孙斌)[1,2,3,†], Yang-Fan He(何阳帆)[2,3], Ruo-Yun Luo(罗若云)[4], Tai-Yang Zhang(章太阳)[5], Qiang Zhou(周强)[4,6], Shao-Yi Wang(王少义)[2,3], Du Wang(王度)[7], and Zong-Qing Zhao(赵宗清)[2,‡]

[1] *Department of Plasma Physics and Fusion Engineering, Key Laboratory of Geospace Environment (Chinese Academy of Sciences), University of Science and Technology of China, Hefei* 230026, *China*

[2] *Laser Fusion Research Center, China Academy of Engineering Physics (CAEP), Mianyang* 621900, *China*

[3] *The Sciences and Technology on Plasma Physics Laboratory, CAEP, Mianyang* 621900, *China*

[4] *Institute of Fundamental and Frontier Sciences, University of Electronic Science and Technology of China, Chengdu* 610054, *China*

[5] *Department of Nuclear, Plasma, and Radiological Engineering, University of Illinois at Urbana-Champaign, 104 South Wright Street, Urbana, IL* 61801, *USA*

[6] *CAS Key Laboratory of Quantum Information, University of Science and Technology of China, Hefei* 230026, *China*

[7] *The Institute of Technological Sciences, Wuhan University, Wuhan* 430072, *China*

(Received 7 January 2023; revised manuscript received 1 June 2023; accepted manuscript online 7 June 2023)

Dielectric laser accelerators (DLAs) are considered promising candidates for on-chip particle accelerators that can achieve high acceleration gradients. This study explores various combinations of dielectric materials and accelerated structures based on the inverse Cherenkov effect. The designs utilize conventional processing methods and laser parameters currently in use. We optimize the structural model to enhance the gradient of acceleration and the electron energy gain. To achieve higher acceleration gradients and energy gains, the selection of materials and structures should be based on the initial electron energy. Furthermore, we observed that the variation of the acceleration gradient of the material is different at different initial electron energies. These findings suggest that on-chip accelerators are feasible with the help of these structures and materials.

Keywords: dielectric laser accelerator, high gradient accelerator, inverse Cherenkov effect, accelerated structure and material

PACS: 41.75.Jv, 41.20.Jb, 42.25.–p, 41.20.–q **DOI:** 10.1088/1674-1056/acdc0a

1. Introduction

Particle accelerators have been used for a variety of purposes beyond basic research since their invention in the 20th century.[1,2] They have been instrumental in advancing many fields including material science, solid state physics, biology, chemistry, geology, and archaeology, as well as industrial, agricultural, and medical applications. However, traditional radio-frequency (RF) accelerators are often large, heavy, and expensive due to the low breakdown threshold of metallic structures and power limitations of microwave sources.[3–6] This has led researchers to explore more affordable and compact accelerating solutions.[7–13]

One such solution is the dielectric laser accelerators (DLAs), which is based on laser-dielectric material interaction and has attracted increasing interest in recent years.[14–20] DLAs can achieve acceleration gradients exceeding 1 GV/m, which is significantly higher than those in conventional accelerators.[21–23] It has the potential to revolutionize electron microscopes, colliders, and attosecond particle, and radiation sources.[24–26] In DLAs, particles (usually electrons) can be accelerated by designing dielectric materials to modulate the incident laser. Thus, an important research direction is selecting materials and designing structures for laser modulation in DLAs.

The current DLAs is mainly based on the inverse Smith–Persell effect (ISP-DLAs), and there are many accelerated structures based on this theory, such as various common grating or photonic crystal accelerated structures.[27–29] However, in the current research, ISP-DLAs has encountered some challenges. For instance, the accelerated structures need to be prepared by advanced micro and nano processing techniques; they also need to be fabricated using dielectric materials with high laser damage threshold, usually SiO_2, due to its mature micro and nano processing means. At the same time, materials such as Al_2O_3, which have higher laser damage threshold but cannot be micro-nano-processed, cannot be applied. Furthermore, the laser damage threshold of the micro-nano-processed structures will be reduced, which will further limit the acceleration gradient. Additionally, long-range acceleration faces many problems, such as phase matching, energy utilization efficiency, and the need for laser pulse front tilting techniques. To address these challenges, researchers have proposed an alternative approach based on the inverse Cherenkov effect (ICA-DLAs). However, the current ICA-DLAs is still in

†Corresponding author. E-mail: binsun97@mail.ustc.edu.cn
‡Corresponding author. E-mail: zhaozongqing99@caep.cn

© 2023 Chinese Physical Society and IOP Publishing Ltd

its infancy, with relatively few structures and materials used, a lack of optimization studies on structures, and the need to explore other materials with high laser damage thresholds.[30–34]

Our study proposes several dielectric laser accelerator (DLAs) structures based on the inverse Cherenkov effect, and we compare four materials using simulations. Our designs are experimentally feasible and enhance the acceleration gradient and energy gain compared to earlier ICA-DLAs structures. They are suitable for accelerating electrons from sub-relativity to the relativistic state. These structures are also straightforward and require less processing, making it possible to use a wider range of materials compared to ISP-DLAs structures.[27] Our research findings will contribute to future studies on compact accelerators, and researchers can leverage these structures and materials to achieve larger acceleration gradients.

2. Accelerator simulation design

Figure 1 illustrates the three primary structures analyzed in this study. The structures are designed with two laser beams that strike the prism's surface vertically and simultaneously from both sides, while the electron beam advances along the x axis in a vacuum channel. Structure A, depicted in Fig. 1(a), employs a dielectric prism with an inverted right triangle cross-section. Structure B, illustrated in Fig. 1(b), uses a prism with a right triangular cross-section. Structure C, shown in Fig. 1(c), has a parallelogram cross-section. Figure 1(d) depicts the correspondence of the three structures. The length of the bottom edge of all three structures is L, the angle between the left beveled edge and the bottom edge is α, and the angles between the right beveled edge and the bottom edge are θ_1, θ_2, and θ_3, respectively. The angles satisfy the relations $\theta_1 = \pi/2 - \alpha$, $\theta_2 = \pi/2$, and $\theta_1 = \pi - \alpha$. As a result, the structures under the structure A evolved into structures B and C, respectively.

To investigate the acceleration of electrons, two-dimensional three-velocity (2D3V) simulations based on finite-element-method (FEM) and particle-in-cell (PIC) algorithms were employed. The electric field strength was set to $E_0 = 6$ GV/m, and the laser wavelength was selected as 800 nm, which is the most widely wavelength for DLAs studies. In the simulation, continuous-wave (CW) mode was employed. The vacuum channel had a length of $L = 10\lambda$ and a width of $C = \lambda/4$, which was suggested in a prior DLAs study.[27,28] The angle α was given by $\alpha = \arcsin(1/n\beta)$. The initial kinetic energy of the electrons injected in the simulations spanned from 300 keV to 1000 keV, and β was the relativistic velocity corresponding to the energy. This energy interval was chosen because after higher than 1000 keV, β does not change much and therefore the structure does not change much; while below 300 keV, the corresponding pinch angle α for some materials is too high and basically unsuitable for acceleration. The monoenergetic electron beam's charge was approximately 10.7 fC, and there was no initial energy spread. With a spatially KV distribution, the initial longitudinal beam length equates to 0.27 fs and the initial transverse dimension was 0.16 μm. The KV distribution placed particles uniformly in phase space. The distance between particles was roughly the same throughout the beam. The initial normalized emittance was 10^3 pm·rad. Four materials were used in this study, and the material refractive indices used in the simulations were divided into $n_{SiO_2} = 1.45$, $n_{Al_2O_3} = 1.76$, $n_{Y_2O_3} = 1.91$, and $n_{ZnO_2} = 2.14$.[35–38]

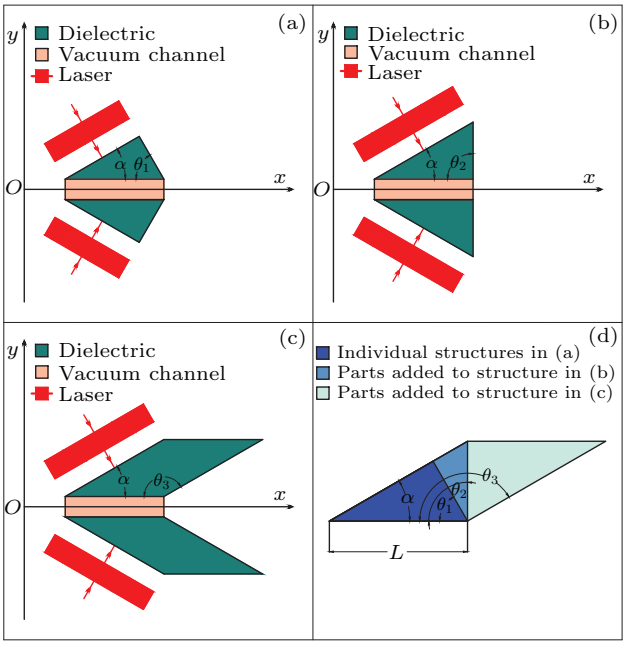


Fig. 1. Schematic diagrams of the cross sections of the three main structures studied and comparisons. In (a)–(c), the dielectric structure is depicted in green, the vacuum channel that accelerates electrons within the dielectric structure is depicted in orange, and the laser is depicted in red. Structure A has a right triangle with its cross section flipped, while structure B has a standard right triangle. Structure C has a parallelogram. The comparison of the three individual structures is shown in panel (d), where dark blue designating structure A, light blue designating the portion added to structure B relative to structure A, and blue–green designating the portion added to structure C relative to structure B.

3. Simulation results and discussion

Figure 2(a) illustrates how the acceleration gradient changes as electron energy changes for various materials and structural configurations. First, for all three configurations of the four materials, the acceleration gradient rises as electron energy rises. This is because when the electron energy increases, the structural pinch angle reduces, and earlier studies have shown that the pinch angle may be decreased to enhance the acceleration gradient.[30,31,34] Second, with $G_B \approx G_C \geq G_A$, the acceleration gradients of the B and C structures are comparable and both are higher than the acceleration gradient of the A structure.

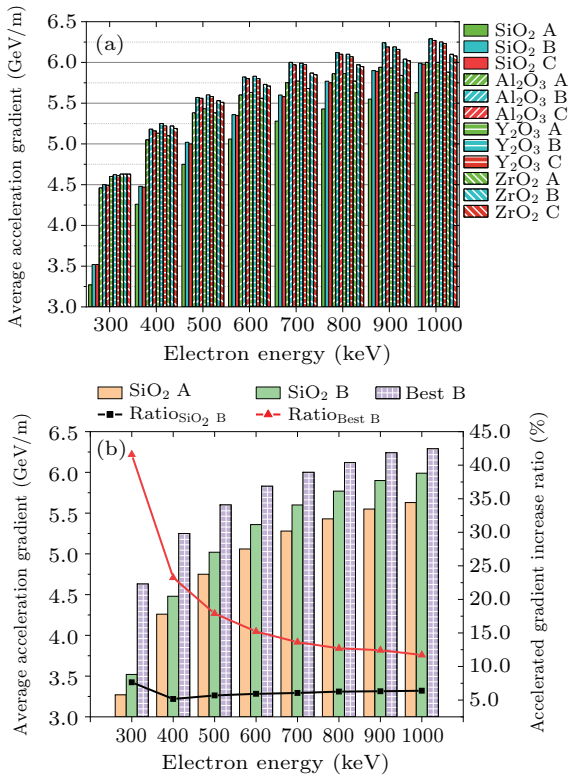


Fig. 2. (a) After the combination of four materials and three structures, the acceleration gradient varies depending on the energy of the input electron in each scenario. Structures A, B, and C are represented by the hues dark green, vivid blue, and red, respectively. The horizontal transverse stripe, oblique down-left stripe, oblique down-right stripe, and unshaded pattern all stand for SiO_2, Al_2O_3, Y_2O_3, and ZrO_2, respectively. (b) The results of the accelerated gradients of the best materials utilizing Y_2O_3 and Al_2O_3, respectively, with the combination of B structures at each interval. The accelerated gradients of the combination of A and B structures of SiO_2 materials. SiO_2 and structure A's acceleration gradient is represented by the color orange, SiO_2 and structure B's acceleration gradient is represented by the color light green, and the acceleration gradient for the best material and structure B is represented by the color purple with a square pattern. The improvement of the SiO_2 and structure B combination over the SiO_2 and structure A combination is shown by the black line with a square in it. The improvement of the best material and structure B combination is depicted by the red line with the triangle in it.

This is due to the disordered electric field caused by structure A's left-side boundary effect and the existence of θ_1 (acute angle). Structure A is the same as the left side of structure B and structure C. The problem of structure A arises from the difference in the right side. First, because the right side of structure A is downward slanted to the left, resulting in the laser on the bottom surface being fully reflected back to the slant, part of the laser will be reflected back to the bottom surface, and the electric field on the bottom surface superposes, affecting the amplitude and phase of the accelerating field on the bottom surface, thus affecting the acceleration of electrons; second, the right side of structure A has a sharp acute angle, which will lead to field disorder in the vicinity of this acute angle. In addition, in the actual process, the sharp angle configuration will increase processing difficulty, and the enhanced field here will make the medium easier to be penetrated by the electric field, meaning that the actual acceleration of the laser intensity will be lower in structure A compared to structure B. Furthermore, there is not much of a difference between structures B and C, in some cases, structure B may even be better. This suggests that structure B, which has a smaller structure and an easier-to-process form, can address some of the issues with structure A.

The effect of material on the acceleration gradient is compared for all the same structures. SiO_2 has a smaller acceleration gradient than the other three materials. At lower energy (300 keV–600 keV), $G_{Y_2O_3} > G_{ZrO_2} > G_{Al_2O_3}$, and at higher energy (700 keV–1000 keV), $G_{Al_2O_3} > G_{Y_2O_3} > G_{ZrO_2}$. These variations result from the fact that, as the refractive index increases, the angle decreases, making it possible to raise the ratio of the dielectric electric field strength to the accelerated electric field strength in the vacuum channel. However, as the refractive index increases, the transmittance decreases and the electric field strength in the dielectric decreases, resulting in a decrease in the electric field strength in the vacuum channel. Therefore, greater refractive indexes are not necessarily better, and models and calculations must be used to determine the ideal dielectric material. To obtain the maximum acceleration gradient, the appropriate dielectric material must be chosen based on the size of the electron energy.

The enhancement of the acceleration gradient is improved under structures B and C made of different materials in comparison to that under structure A made of corresponding material. The acceleration gradient can be raised for all materials by changing the structure, but for SiO_2 materials, especially at 300 keV, where the large pinch angle is present, the acceleration gradient can be raised to the greatest extent. The results of the combination of the best material (using Y_2O_3 or Al_2O_3, respectively) with the B structure at each interval are shown in Fig. 2(b), along with the acceleration gradients based on the combination of the A and B structures of SiO_2 material. Additionally, it displays the gradients of acceleration for the combinations of SiO_2 and structure A as a benchmark, SiO_2 and structure B, and optimum material and structure B, respectively. SiO_2 and the structure A are the material and structure most frequently employed. The acceleration gradient can be increased by up to 41.6% with the combination of the best material and the structure B, or an acceleration gradient of 4.6 GeV/m, while the least enhancement is 11.7%, or an acceleration gradient of 6.3 GeV/m. Meanwhile, an improvement of up to 7.6% and a minimum of 5.2% can be made even without changing the material by switching the structure to a B structure. In addition, SiO_2 has no advantage over other materials in terms of acceleration, but it is a common DLAs material, due to the fact that materials such as Al_2O_3 cannot be finely processed as SiO_2. All three structures compared in this article do not require fine processing, thus contributing to the study of DLAs and also giving these materials the opportunity to be used in scenarios.

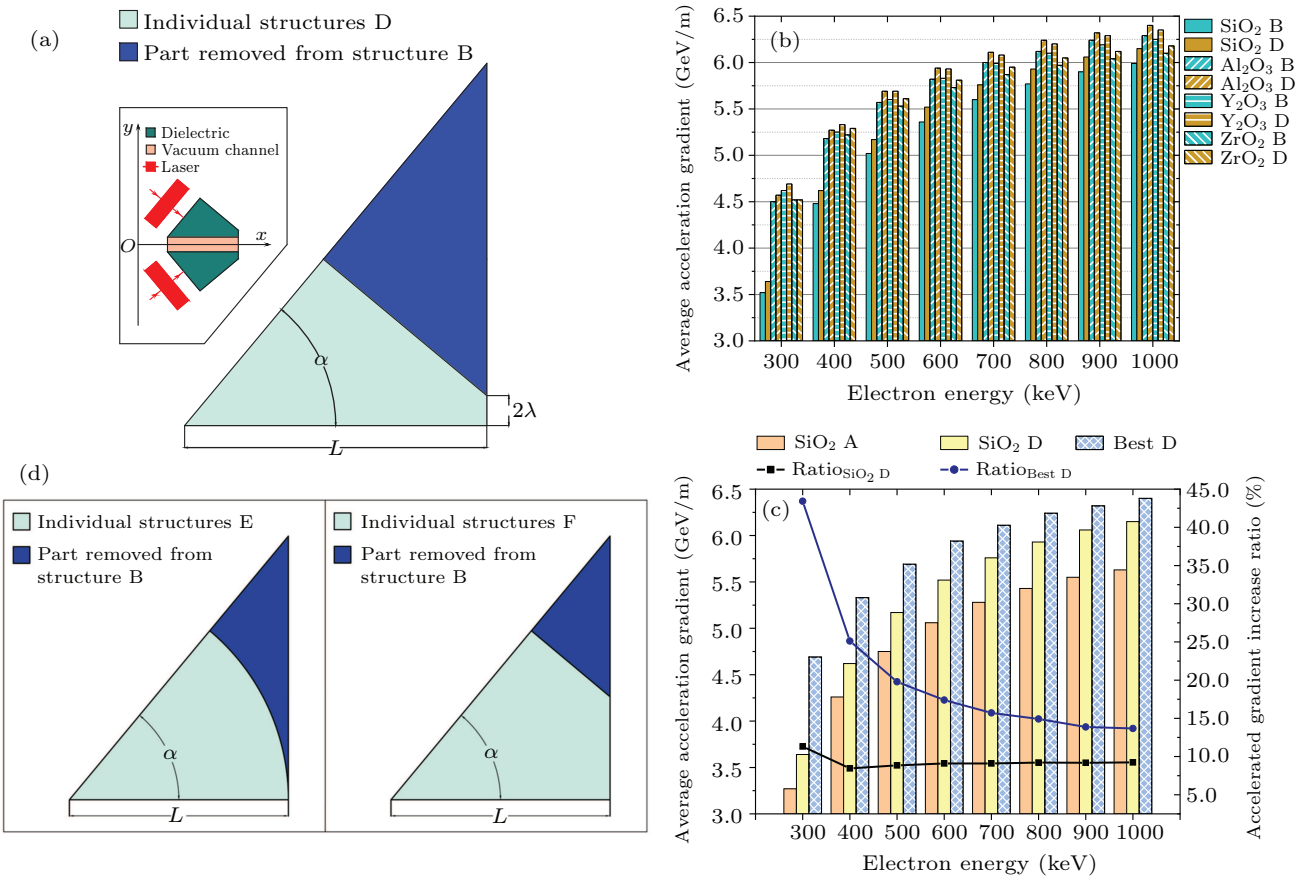


Fig. 3. (a) Schematic diagram of structure D. The original structure D is shown in light blue, while the portion of structure B that was destroyed is shown in dark blue. Figure 1-like whole accelerated design concept is depicted in the drawing attached; (b) The variation in incident electron energy and how it affected the acceleration gradient for each of the four materials and combinations of the two structures. Structure B and structure D are represented by the vivid blue and earthy yellow hues, respectively. The filling designs match the materials as seen in Fig. 2(b). (c) The results of the accelerated gradients of the best materials utilizing Y_2O_3 and Al_2O_3, respectively, with the combination of D structures at each interval. The accelerated gradients of the combination of A and D structures of SiO_2 materials. SiO_2 and structure A's acceleration gradient is represented by the color orange, SiO_2 and structure D's acceleration gradient is represented by the color bright yellow, and the acceleration gradient for the best material and structure D is represented by the color the blue stripe. The improvement of the SiO_2 and structure D combination over the SiO_2 and structure A combination is shown by the black line with a square in it. The improvement of the best material and structure D combination is depicted by the blue line with the circle in it; (d) The left and right diagrams show the schematic diagrams of structure E and structure F, respectively.

Additionally, the upgraded structure using the structure B as the fundamental model was also researched for comparison because of its superiority over the other two structures. The three structures shown in Figs. 3(a) and 3(d) provide the best results. Structure D is based on structure B in Fig. 3(a). Only two incident laser wavelength lengths are present on the right vertical side, and similarly to how structure A was handled, a vertical line is drawn on the opposite side. These two incident laser wavelength lengths were used because, following extensive simulation optimization, this was the best outcome. The right side of the left side structure E in Fig. 3(d) is treated by circularizing it, with the radius being equal to the length L of the bottom edge and the center being the vertex of the angle. The right-hand structure F in Fig. 3(d) is a symmetric structure with both the beveled edge and the lower bottom edge L. The right-hand vertical edge is the same length as the upper bottom edge, and both sides are perpendicular to the lower bottom edge and the beveled edge, respectively.

The accelerated gradient results for the four materials in the structure D are shown in Fig. 3(b). The acceleration gradient of the structure D is stronger than that of the structure B, and the difference caused by the material is also consistent with Fig. 2. Using the combination of SiO_2 and structure A as a benchmark, figure 3(c) illustrates the enhanced magnitude of the combination of SiO_2 and structure D as well as the combination the of optimum material and D structure. The results show that the highest acceleration gradient enhancement, which corresponds to an acceleration gradient of 4.69 GeV/m, can be reached by the combination of the optimal material and D structure. The lowest acceleration gradient enhancement corresponds to an acceleration gradient of 6.40 GeV/m. While maintaining the same material, replacing the structure with a D structure can result in an enhancement of up to 11.3% and as little as 8.5%.

4. Conclusion and perspectives

In summary, this article investigates six structures and four materials for use in dielectric laser acceleration based on

the inverse Cherenkov effect in the energy range from 300 keV (subrelativity) to 1000 keV (relativity). The investigation reveals that the structure with the largest average acceleration gradient among them is the combination of optimum material and D structure. This study also provides the best among the four materials for various initial electron energies, which can serve as a foundation for choosing materials for subsequent laser dielectric acceleration investigations. Furthermore, this study demonstrates that by utilizing the ideal mixture of materials and structures, larger acceleration gradients and energy gains can be obtained. These findings will serve as a starting point for future research on-chip accelerator structures in subrelativity to relativity acceleration.

Acknowledgements

The authors thank Dr. Bin Zhang of Tel Aviv University, Dr. Wei Li of the University of Science and Technology of China, and Dr. Lai Wei of Laser Fusion Research Center, CAEP, for the insightful discussion.

Project supported by the National Natural Science Foundation of China (Grant No. 11975214).

References

[1] Zhang Y, Fang W C, Huang X X, Tan J H, Wang C, Wang C P and Zhao Z T 2021 *Nucl. Sci. Tech.* **32** 38
[2] Fu G Y, Dang Y L, Liu F L, Wu D, He C Y and Wang N Y 2019 *Chin. Phys. B* **28** 060707
[3] Chen S, Hao J K, Lin L, Zhu F, Feng L W, Wang F, Xie H M, Guo X, Chen M, Quan S W and Liu K X 2018 *Chin. Phys. Lett.* **35** 037401
[4] Yang Z, Huang S, He Y, Lu X, Guo H, Li C, Niu X, Xiong P, Song Y, Wu A, Xie B, You Z, Chu Q, Tan T, Pan F, Lu M, Luo D, Zhang J, Zhang S and Zhan W 2021 *Chin. Phys. Lett.* **38** 092901
[5] Xiao O Z, Fukuda S, Zhou Z S, Zaib U N, Wang S C, Lu Z J, Pei G X, Iqbal M and Dong D 2022 *Chin. Phys. B* **31** 088401
[6] Geng P F, Chen M, An X Y, Liu W Y, Zhu X Z, Li J L, Li B Y and Sheng Z M 2023 *Chin. Phys. B* **32** 044101
[7] Geng P F, Lv W J, Li X L, Tang R A and Xue J K 2018 *Chin. Phys. B* **27** 035201
[8] Deng S and Liu M 2019 *Chin. Phys. B* **28** 044101
[9] Hu Y N, Cheng L H, Yao Z W, Zhang X B, Zhang A X and Xue J K 2020 *Chin. Phys. B* **29** 084103
[10] Naranjo B, Valloni A, Putterman S and Rosenzweig J B 2012 *Phys. Rev. Lett.* **109** 164803
[11] Peralta E A, Soong K, England R J, Colby E R, Wu Z, Montazeri B, McGuinness C, McNeur J, Leedle K J, Walz D, Sozer E B, Cowan B, Schwartz B, Travish G and Byer R L 2013 *Nature* **503** 91
[12] England R J, Noble R J, Bane K, Dowell D H, Ng C K, Spencer J E, Tantawi S, Wu Z, Byer R L, Peralta E, Soong K, Chang C M, Montazeri B, Wolf S J, Cowan B, Dawson J, Gai W, Hommelhoff P, Huang Y C, Jing C, McGuinness C, Palmer R B, Naranjo B, Rosenzweig J, Travish G, Mizrahi A, Schachter L, Sears C, Werner G R and Yoder R B 2014 *Rev. Mod. Phys.* **86** 1337
[13] Leedle K J, Pease Fabian R, Byer R L and Harris J S 2015 *Optica* **2** 158
[14] Wootton K P, Wu Z, Cowan B M, Hanuka A, Makasyuk I V, Peralta E A, Soong K, Byer R L and England Joel R 2016 *Opt. Lett.* **41** 2696
[15] McNeur J, Kozák M, Schönenberger N, Leedle K J, Deng H, Ceballos A, Hoogland H, Ruehl A, Hartl I, Holzwarth R, Solgaard O, Harris J S, Byer R L and Hommelhoff P 2018 *Optica* **5** 687
[16] Yousefi P, Schönenberger N, McNeur J, Kozák M, Niedermayer U and Hommelhoff P 2019 *Opt. Lett.* **44** 1520
[17] Sapra Neil V, Yang Ki Y, Vercruysse D, Leedle Kenneth J, Black Dylan S, England R J, Su L, Trivedi R, Miao Y, Solgaard O, Byer R L and Vučković J 2020 *Science* **367** 79
[18] Shiloh R, Illmer J, Chlouba T, Yousefi P, Schönenberger N, Niedermayer U, Mittelbach A and Hommelhoff P 2021 *Nature* **597** 498
[19] Meng Y, Chen Y, Lu L, Ding Y, Cusano A, Fan J A, Hu Q, Wang K, Xie Z, Liu Z, Yang Y, Liu Q, Gong M, Xiao Q, Sun S, Zhang M, Yuan X and Ni X 2021 *Light Sci. Appl.* **10** 235
[20] Chlouba T, Shiloh R, Forsberg P, Hamberg M, Karlsson M, Kozák M and Hommelhoff P 2022 *Opt. Express* **30** 505
[21] Plettner T, Byer R L and Montazeri B 2011 *J. Mod. Opt.* **58** 1518
[22] Breuer J, McNeur J and Hommelhoff P 2014 *J. Phys. B. At. Mol. Opt. Phys.* **47** 234004
[23] Cesar D, Maxson J, Musumeci P, Shen X, England R J and Wootton K P 2018 *Nucl. Instrum. Meth. A* **909** 252
[24] Chen L, Lu X, Li D and Li Y 2018 *Chin. Phys. B* **27** 074101
[25] Fu X W, Wang E, Zhao Y, Liu A, Montgomery E, Gokhale V J, Gorman J J, Jing C, Lau J W and Zhu Y 2020 *Sci. Adv.* **6** eabc3456
[26] Zheng D, Huang S, Zhu C, Li Z, Zhang Y, Yang D, Tian H, Li J, Yang H and Li J 2022 *Nanoscale* **14** 10477
[27] Plettner T, Lu P P and Byer R L 2006 *Phys. Rev. ST Accel. Beams* **9** 111301
[28] Aimidula A, Bake M A, Wan F, Xie B S, Welsch C P, Xia G, Mete O, Uesaka M, Matsumura Y, Yoshida M and Koyama K 2014 *Phys. Plasmas* **21** 023110
[29] He Y F, Sun B, Ma M J, Li W, He Q Y, Cui Z H, Wang S Y and Zhao Z Q 2022 *Nucl. Sci. Tech.* **33** 120
[30] Kozák M, Beck P, Deng H, McNeur J, Schönenberger N, Gaida C, Stutzki F, Gebhardt M, Limpert J, Ruehl A, Hartl I, Solgaard O, Harris J S, Byer R L and Hommelhoff P 2017 *Opt. Express* **25** 19195
[31] Liu W, Yu Z, Sun L, Liu Y, Jia Q, Xu H and Sun B 2020 *Phys. Rev. Appl.* **14** 014018
[32] Sun L, Liu W, Zhou J, Zhu Y, Yu Z, Liu Y, Jia Q, Sun B and Xu H 2021 *New J. Phys.* **23** 063031
[33] Liu W, Sun L, Yu Z, Liu Y, Jia Q, Sun B and Xu H 2021 *Opt. Lett.* **46** 4398
[34] Sun B, He Y F, Luo R Y, Zhang T Y, Zhou Q, Wang S Y, Zheng J and Zhao Z Q 2023 *Nucl. Sci. Tech.* **34** 23
[35] Malitson I H 1965 *J. Opt. Soc. Am.* **55** 1205
[36] Malitson I H 1962 *J. Opt. Soc. Am.* **52** 1377
[37] Nigara Y 1968 *Jpn. J. Appl. Phys.* **7** 404
[38] Wood D L and Nassau K 1982 *Appl. Opt.* **21** 2978